VesSAM: Efficient Multi-Prompting for Segmenting Complex Vessel

Suzhong Fu^{1,2}, Rui Sun^{1,2}, Xuan Ding^{1,2}, Jingqi Dong^{1,2}, Yiming Yang^{1,2}, Yao Zhu³, Min Chang Jordan Ren⁴, Delin Deng⁵, Angelica Aviles-Rivero⁶, Shuguang Cui^{1,2}, Zhen Li^{1,2,*}

¹FNii-Shenzhen, CUHK-Shenzhen, Shenzhen, China

Abstract—Accurate vessel segmentation is critical for clinical applications such as disease diagnosis and surgical planning, yet remains challenging due to thin, branching structures and low texture contrast. While foundation models like the Segment Anything Model (SAM) have shown promise in generic segmentation, they perform sub-optimally on vascular structures. In this work, we present VesSAM, a powerful and efficient framework tailored for 2D vessel segmentation. VesSAM integrates (1) a convolutional adapter to enhance local texture features, (2) a multi-prompt encoder that fuses anatomical prompts-including skeletons, bifurcation points, and segment midpoints-via hierarchical cross-attention, and (3) a lightweight mask decoder to reduce jagged artifacts. We also introduce an automated pipeline to generate structured multi-prompt annotations, and curate a diverse benchmark dataset spanning 8 datasets across 5 imaging modalities. Experimental results demonstrate that VesSAM consistently outperforms state-of-the-art PEFT-based SAM variants by over 10% Dice and 13% IoU, and achieves competitive performance compared to fully fine-tuned methods. with significantly fewer parameters. VesSAM also generalizes well to out-of-distribution (OoD) settings, outperforming all baselines in average OoD Dice and IoU.

Index Terms—vascular segmentation, segment anything model, multi-prompts fusion, information fusion

I. INTRODUCTION

Accurate segmentation of vascular structures is vital for clinical applications such as disease diagnosis, surgical planning, and treatment monitoring. Unlike solid organs, vessels display thin, elongated geometries with complex branching patterns, posing unique challenges for automatic segmentation. While deep learning-based methods have shown success in vessel segmentation [4], [15]–[19], they often rely on dense pixel-wise annotations, which are expensive and time-consuming to obtain in clinical workflows.

Recently, foundation models such as the Segment Anything Model (SAM) [30] have enabled prompt-based, domain-adaptable segmentation. In the medical domain, SAM-based extensions [31]–[34] have demonstrated promising results for organ and tumor segmentation. These models use generic prompts—such as boxes or sparse points—to guide segmentation, reducing annotation burden. However, their performance on vessel segmentation remains unsatisfactory.

As illustrated in Fig. 1, standard prompting strategies are sufficient for simple vascular cases. For example, box-by-

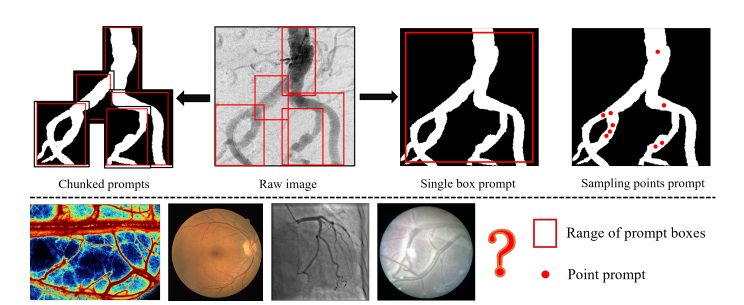


Fig. 1: Motivating examples showing the limitations of conventional prompt strategies in vessel segmentation. Simple structures can be handled by boxes or random points, but these methods fail on complex, dense vascular networks—highlighting the need for more informative, structure-aware prompting.

box annotation or random point sampling within a mask can reasonably segment coarse, tree-like vessels. However, these strategies deteriorate in complex cases. First, fullimage bounding boxes provide no effective spatial constraint—essentially acting as no prompt. Second, random point sampling within non-convex vessel masks often leads to spatial bias and point clustering, resulting in uneven supervision. Most critically, these approaches are ill-suited for fine-grained, high-density vascular networks with intricate bifurcations and low contrast.

The lower row of Fig. 1 illustrates real-world vascular images with high structural complexity. These cases challenge prompt-based methods due to subtle textures, blurred boundaries, and variable morphology across imaging modalities. In such scenarios, traditional prompts either fail to provide sufficient anatomical guidance or lack the resolution to preserve fine vessel continuity. This highlights the need for more specialized and information-rich prompts that align with vascular topology.

Beyond prompting, model architecture also constrains performance. Existing SAM-based frameworks rely heavily on ViT backbones. While transformers excel at modeling longrange dependencies, their patch-based tokenization can neglect local texture continuity—especially in non-convex, sparse

²School of Science and Engineering, CUHK-Shenzhen, Shenzhen, China

³Zhejiang University, Hangzhou, China ⁴Boston University, United States

⁵Vanderbilt University, United States ⁶Tsinghua University, Beijing, China

structures like vessels. In organ segmentation, patch-wise attention aligns well with intra-mask continuity, but in vessel segmentation, masks often span multiple disconnected or narrow regions, undermining global modeling alone. Therefore, a successful vessel segmentation system must integrate both global context and local detail through texture-sensitive and topologically meaningful representations.

To address these challenges, we propose VesSAM—a structure-aware and parameter-efficient segmentation framework tailored specifically for vessels. VesSAM introduces three core innovations: (1) a convolutional adapter that augments ViT with localized texture sensitivity while supporting efficient fine-tuning; (2) a multi-prompt encoder that processes diverse anatomical prompts—including skeleton maps, bifurcation points, and segment midpoints—via hierarchical cross-attention and graph reasoning; and (3) a lightweight mask decoder that mitigates jagged boundaries using coarse-to-fine upsampling. To support this framework, we construct a multi-modality vessel dataset enriched with automatically generated prompt annotations, providing a foundation for structure-aware training. To facilitate research and reproducibility, our code is publicly available.

1

Our key contributions are as follows:

- We propose VesSAM, a segmentation framework that enhances ViT-based encoders with localized texture modeling and anatomical prompt fusion, significantly improving accuracy on non-convex vascular structures.
- We design a multi-prompt encoder that unifies sparse (e.g., bifurcation points) and dense (e.g., skeletons, masks) anatomical cues using hierarchical cross-attention and graph-based topology reasoning.
- We introduce a **convolutional adapter** that improves fine-detail representation while enabling parameter-efficient tuning via LoRA-style isolation.
- We develop an automated prompt generation pipeline and release a benchmark dataset spanning eight vascular datasets across five imaging modalities, supporting scalable, high-fidelity supervision.

II. DATASETS

Most SAM-related medical segmentation methods focus on large convex organs, where sparse prompts (e.g., bounding boxes or random points) are often sufficient. However, these strategies are inadequate for segmenting **non-convex and topologically complex structures** such as blood vessels, where global spatial prompts lack the fine-grained details granularity and connectivity prompts.

Multi-Prompt Strategy. We design three anatomically grounded prompt types to guide vascular segmentation: Bifurcation points: minimal keypoints to resolve topological ambiguity; Segment midpoints: orientation-aware anchors that reduce redundancy; Skeleton maps: structural templates that preserve global vessel continuity.

Algorithm 1 Multi-Prompt Generator for Vessel Analysis

Input: image I, vessel mask M, degree computation kernel K, distance threshold δ

Output: Skeleton map S, Bifurcation points B, Segment midpoints P

- 1: $S \leftarrow \text{Skeletonization}(M)$ // Extract the skeleton
- 2: $D \leftarrow S * K$ // Compute degree of each skeleton point
- 3: $B \leftarrow \{p \mid D(p) \ge 3\}$ // Select bifurcation points
- 4: Partition S using B // Get isolated vessel segments
- 5: for each vessel segment V_i in segmented S do
- 6: $P_i \leftarrow \text{Midpoint}(V_i)$
- 7: end for
- 8: $B \leftarrow RemoveClosePoints(B, \delta)$
- 9: $P \leftarrow RemoveClosePoints(\cup P_i, \delta)$ // Filter close points
- 10: **return** S, B, P

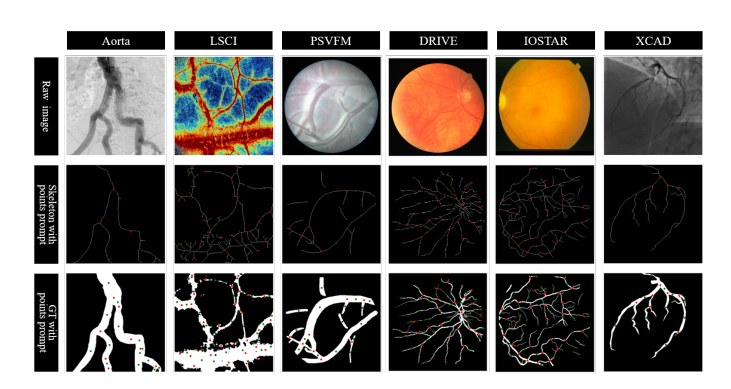


Fig. 2: Examples from different datasets. Top row: raw vessel images; middle row: skeletons with bifurcation points (red) and midpoints (green); bottom row: final segmentation masks with prompt annotations.

To address this limitation, we construct a comprehensive vessel benchmark by aggregating **eight datasets across five imaging modalities**, each annotated with precise vessel delineations. Specifically, the dataset includes pelvic-iliac artery angiograms (Aorta) [8], coronary XCAD [9], retinal datasets (ARIA [10], DRIVE [11], HRF [12], IOSTAR [13]), placental vessel images (PSVFM) [14], and laser speckle contrast imaging (LSCI) [16]. All samples are provided with expert-validated ground truth annotations.

To systematically extract these prompts, we develop an automatic prompt generation algorithm, shown in Algorithm 1, which processes vessel masks to generate informative prompt sets. The pipeline includes skeletonization, bifurcation detection via degree computation, and segment partitioning for midpoint extraction. Redundant points are removed based on a configurable distance threshold to ensure spatial diversity and information density.

As illustrated in Fig. 2, these prompt types effectively encode vascular topology. Skeletons represent global connectivity, while bifurcation and midpoint prompts highlight local structure. These features are highly informative and generalizable across vessel types.

¹https://github.com/VersaceSu/VesSAM

To reduce annotation costs and enable fast domain adaptation, we develop **visual drawing and automated annotation generation tools** that generate multi-prompt labels from rough scribbles or binary masks (as illustrated in Fig. 3 pink area). This pipeline not only streamlines annotation for unfamiliar datasets but also supports model training in low-supervision or few-shot scenarios.

III. RELATED WORKS

Recent advances in foundational models, prompt-based segmentation, and vascular imaging have significantly reshaped the medical image analysis landscape. In this section, we review relevant developments across three major dimensions: foundation models in medical tasks, parameter-efficient finetuning techniques, and vessel segmentation methods.

A. Foundational Models in Medical Tasks

Foundation models [20]–[24]—including large-scale transformers and vision-language architectures—have shown strong generalization across modalities. Pretrained language models such as BioBERT [44] and MedGPT [45] have improved performance on various clinical NLP tasks, while multimodal models like CLIP [25] and LLaVa [43] enable image-report alignment and cross-modal reasoning.

In vision tasks, the Segment Anything Model (SAM) [30] enables zero-shot segmentation via prompt-based supervision. Extensions such as MedSAM [31] and SAM-Med2D [33] adapt SAM to medical images using large-scale annotated datasets for organs and tumors. However, these adaptations still struggle with thin, low-contrast structures like blood vessels.

B. Parameter-Efficient SAM Fine-Tuning

To reduce the computational overhead of fine-tuning large models, parameter-efficient fine-tuning (PEFT) methods have been proposed [41], [42]. Approaches such as LoRA [38] and Visual Prompt Tuning [39] allow adaptation by updating a small subset of parameters. In medical imaging, methods like SAMed [32] and SAM-Med2D [33] integrate LoRA and adapter modules into SAM, enabling segmentation with <5% trainable parameters.

Further improvements have been made through prompt engineering and cross-modal alignment, which enhance flexibility across imaging domains. Despite these advances, most existing PEFT approaches focus on large, coarse structures and are less effective for fine-grained, topology-sensitive tasks like vascular segmentation.

C. Vascular Segmentation

Vessel segmentation remains a particularly challenging task due to fine-scale geometries, frequent bifurcation, low signal-to-noise ratios, and modality-specific appearance variance. Traditional techniques—such as vascularness filters and graph-based tracking—often fail to generalize to complex structures.

Deep learning methods such as nnU-Net [4] and TransUNet [5] significantly improve segmentation performance but

rely on large-scale annotations [1]–[3], [6], [15], [19]. Weakly supervised methods like FURNet [16] alleviate annotation costs by leveraging sparse or noisy labels [17], [18].

More recently, SAM-based methods have been explored for vessel segmentation [30]–[37], but they often under-perform due to their dependence on coarse prompts and insufficient modeling of local texture and vessel continuity.

Summary: Existing approaches either focus on general organ segmentation or rely on overly simplistic prompt types. To address these limitations, our work targets fine-grained, structure-aware vessel segmentation through anatomically informed multi-prompting and a dedicated lightweight PEFT architecture.

IV. METHOD

The proposed VesSAM framework is designed to tackle the challenges of vessel segmentation through a prompt-aware and texture-sensitive architecture. As illustrated in Fig. 3, it comprises three core components: a convolution-enhanced image encoder, a multi-prompt encoder capable of integrating both sparse and dense anatomical cues, and a lightweight mask decoder optimized for fine-structured segmentation. In addition, an automated multi-prompt generator extracts structural prompts—such as skeletons, bifurcation points, and segment midpoints—from raw vessel masks to guide the segmentation pipeline.

A. Image Encoder with Convolutional Adapter

While SAM employs a ViT-based [7] image encoder to captures long-range patch relationships, it is less sensitive to local continuity and texture that thin, non-convex vessels require. In organ segmentation, where convexity and spatially consistent prompts dominate, patch-wise modeling suffices. Vascular structures often span across distant patches without strong internal coherence, and thus require enhanced modeling of local cues beyond patch boundaries.

To enhance local texture sensitivity, we introduce a convolutional adapter module that supplements the ViT encoder. This adapter includes depth-wise separable convolutions for efficient channel attention, enabling the model to emphasize salient feature channels while maintaining low computational cost. In parallel, a spatial attention mechanism is implemented via a downsampling-upsampling convolutional sequence, which captures coarse spatial patterns and restores fine details. By fusing channel and spatial attention, the adapter augments the global modeling capacity of ViT with local structural sensitivity, significantly improving performance on thin, elongated vessel structures without introducing substantial parameter overhead.

B. Multi-Prompt Encoder

VesSAM leverages rich anatomical cues through multitype prompts that include sparse point sets (bifurcations and midpoints), dense maps (skeleton and mask), and topological relationships. These prompts are processed through a dedicated

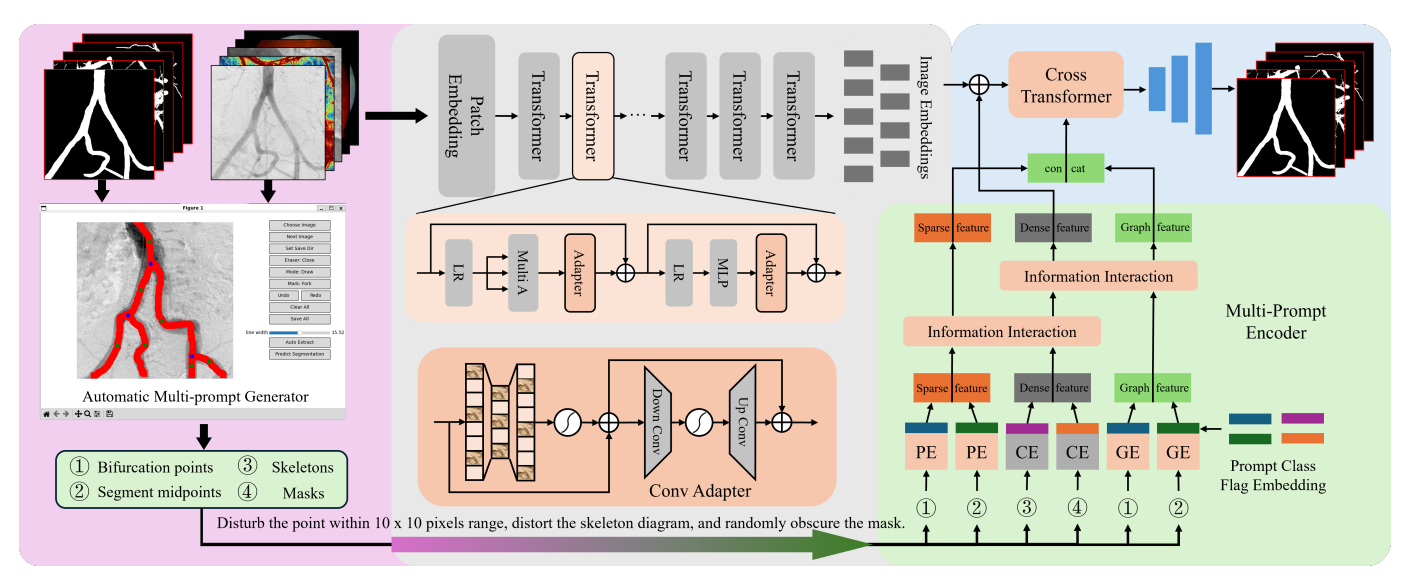


Fig. 3: Overview of the proposed **VesSAM** framework. It comprises four components: an image encoder (gray) enhanced with a convolutional adapter (orange), a multi-prompt encoder (green) for topological prompt fusion, a lightweight mask decoder (blue) for structure-preserving segmentation, and a multi-prompt generator (magenta) for automatic anatomical prompt creation.

encoder designed to preserve their distinct spatial and semantic roles while allowing effective feature fusion.

For sparse prompts, each point set is first embedded with a learnable coordinate encoder and tagged with a prompt-type indicator (e.g., bifurcation or midpoint). The resulting representations are concatenated and passed through a lightweight convolutional block to yield sparse features:

$$SF_i = Conv(Concat(Embed(P_i), Flag_i))$$
 (1)

where $i \in \{branch, mid\}$.

For dense prompts, both the skeleton map and mask are independently encoded through shallow convolutional encoders, producing dense features:

$$\mathbf{DF} = \operatorname{Concat}(\operatorname{Conv}(\mathbf{Sk}), \operatorname{Conv}(\mathbf{Ma}))$$
 (2)

To capture global vessel topology, we additionally construct a graph using the bifurcation and midpoint prompts as nodes, and apply graph convolution to encode their relational structure, resulting in topological features **GF**.

These three sources of information—sparse embeddings (SF), dense maps (DF), and topological priors (GF)—are then integrated via a two-stage cross-attention mechanism. In the first stage, sparse and dense features are fused:

$$SF', DF' = CrossAttention(SF, DF)$$
 (3)

In the second stage, the updated dense features interact with the graph features to yield topology-enhanced representations:

$$GF', DF'' = CrossAttention(DF', GF)$$
 (4)

The outputs \mathbf{SF}' , \mathbf{DF}'' , and \mathbf{GF}' are then forwarded to the mask decoder for final prediction.

C. Lightweight Mask Decoder

The decoder module integrates features from the image encoder and the multi-prompt encoder to produce the final segmentation mask. First, global image tokens extracted by the ViT encoder are concatenated with the prompt features \mathbf{SF}' , \mathbf{DF}'' , and \mathbf{GF}' . Second, the combined sequences processed by a transformer-based attention module for cross-modal fusion.

Unlike SAM's decoder, which relies on transposed convolutions and is susceptible to producing jagged artifacts—especially in texture-rich regions—our design adopts a progressive upsampling strategy. The decoder reconstructs the mask in a coarse-to-fine manner, applying anisotropic Gaussian smoothing at each upsampling stage to mitigate aliasing effects and preserve anatomical continuity. Finally, a lightweight convolutional head outputs the predicted segmentation mask.

Through its modular and prompt-aware design, VesSAM effectively integrates local texture, sparse anatomical landmarks, and global vessel topology. This enables robust segmentation across diverse vascular structures and modalities, pushing forward the goal of generalizable fine-structure segmentation.

V. EXPERIMENTAL SETUP

Implementation Details. All experiments were conducted using PyTorch. The VesSAM model was trained for 75 epochs using the Adam optimizer with an initial learning rate of 1×10^{-4} , which was reduced by a factor of two at the 25th and 50th epochs. Early stopping based on validation loss was employed to avoid overfitting. During the first 50 epochs, we applied data augmentations including point prompt jittering within a 10×10 window, random distortion of the skeleton maps, and partial occlusion of binary masks. To improve robustness in cases where prompts may be missing or noisy, we

TABLE I: Segmentation Performance on 512*512 (H) resolution dataset. The best results are in bold with brown background, and the second-best are underlined.

	PEFT Methods						Full Fine-tuning Methods						
Dataset	VesSAM		SAM-Med2D		SAMed		MedSAM		nnUNet		TransUnet		
Metric	IoU	Dice	IoU	Dice	IoU	Dice	IoU	Dice	IoU	Dice	IoU	Dice	
LSCI	77.10	87.01	61.49	75.73	55.76	70.97	74.15	84.88	82.66	90.43	81.26	89.16	
Placenta	74.38	84.61	56.35	70.58	71.74	82.55	73.86	84.22	69.50	81.03	68.10	79.67	
Retinal	70.10	82.32	24.29	38.91	41.57	58.50	66.03	79.16	60.86	75.58	59.05	74.12	
Aorta	92.33	95.99	84.02	91.26	93.25	96.50	93.06	96.39	93.82	96.78	93.49	96.61	
XCAD	85.54	92.14	47.05	63.62	70.74	82.78	82.42	89.72	71.42	83.23	68.82	81.41	
ALL	78.66	87.36	51.93	64.45	54.01	62.52	76.39	86.08	78.14	86.70	77.19	86.21	
Average(H)	79.89	88.41	54.64	68.02	66.61	78.26	<u>77.90</u>	<u>86.87</u>	75.65	85.41	74.14	84.19	

TABLE II: Performance under OoD setting. The best results are in bold with brown background, and the second-best are underlined. Labeled in the table for testing, and the other four for training.

-	PEFT Methods						Full Fine-tuning Methods						
Dataset	VesSAM		SAM-	SAM-Med2D		SAMed		MedSAM		uuUNet		TransUnet	
Metric	IoU	Dice	IoU	Dice	IoU	Dice	IoU	Dice	IoU	Dice	IoU	Dice	
LSCI	24.27	38.02	8.25	14.48	26.28	40.40	24.77	39.05	27.73	40.99	38.14	51.87	
retinal	50.25	66.76	19.65	32.71	16.27	27.09	10.30	17.89	24.77	38.45	32.30	48.45	
Placenta	23.94	36.99	10.93	17.59	22.20	31.47	0.87	1.67	7.53	12.13	12.32	18.85	
Aorta	80.55	89.10	53.44	68.87	82.07	89.90	34.25	49.01	61.31	75.38	72.74	84.02	
XCAD	61.55	76.16	41.39	58.16	54.81	70.34	30.86	46.89	38.22	53.81	48.06	64.33	
Average	48.11	61.40	26.73	38.36	40.33	51.84	20.21	30.90	31.91	44.15	<u>40.71</u>	53.50	

introduced a stochastic prompt dropout strategy: each prompt type (e.g., bifurcation points, segment midpoints, skeleton maps, or mask regions) was independently omitted with a randomly sampled probability between 0.2 and 0.8 per training batch. This strategy regularizes the model and enhances its generalization to incomplete or sparse annotations.

In-Distribution (ID) and Out-of-Distribution (OoD) Evaluation. We evaluate the proposed framework under both in-distribution (ID) and out-of-distribution (OoD) settings. In the ID setting, each of the eight modality-specific vessel datasets was randomly split into 80% for training and 20% for testing. Additionally, we constructed an aggregated benchmark dataset, denoted as ALL, by combining all modalities under the same 80/20 split. In the OoD setting, we held out one modality as the test domain and trained the model on the remaining modalities. For example, in the wo_LSCI setting, the LSCI dataset is entirely excluded from training and used exclusively for evaluation. This setup simulates real-world scenarios where domain shifts occur between modalities and allows us to rigorously assess VesSAM's cross-domain generalization. Quantitative results are reported in Tables I, and II.

Baseline Methods. To ensure a fair comparison with existing methods, we benchmark VesSAM against five representative baselines. Among them, SAM-Med2D [33], Med-SAM [31], and SAMed [32] represent parameter-efficient fine-tuning (PEFT) extensions of the Segment Anything Model (SAM) and are adapted to the vascular domain with lightweight adapters or LoRA modules. We also include two fully fine-tuned state-of-the-art methods: nnUNet [4] and TransUNet [5], which serve as strong supervised baselines in medical image segmentation. All methods are fine-tuned on the same training splits and evaluated under identical settings.

Ablation Studies. To analyze the contribution of each component in VesSAM, we conducted comprehensive ablation

studies. We evaluated the impact of different prompt combinations by testing six configurations: using only bifurcation points, only segment midpoints, only skeleton maps, bifurcation+midpoints, bifurcation+skeletons, and all three combined. These experiments were performed under 512×512 input resolutions, as shown in Fig. 5.We also validate the effectiveness of the proposed cross-feature fusion mechanism, we tested four configurations: no fusion, fusion between sparse and dense features (SD), fusion between dense and graph features (DG), and combined SD+DG fusion. Results across five single-modality datasets and the aggregated dataset are illustrated in Fig. 6(a). Lastly, we ablated the proposed random prompt dropout strategy by comparing two setups on the full 256×256 dataset: one with random omission of prompts during training, and one with all prompts always present. As shown in Fig. 6(b), incorporating stochastic dropout yields more robust performance in prompt-sparse environments.

VI. RESULTS

Performance under In-Distribution (ID) Settings. We evaluated at 512×512 resolution datasets, VesSAM exhibits even stronger performance. As shown in Table I, the model not only outperforms SAMed by more than 10% in Dice and 13% in IoU, but also surpasses nnUNet by 3% in Dice score. The advantage becomes especially pronounced on datasets such as LSCI and Retina, which require fine-grained boundary preservation and vascular continuity. The multi-prompt mechanism is particularly effective in suppressing noise, preserving thin structures, and improving segmentation robustness. VesSAM also yields strong results on PSVFM and XCAD datasets, highlighting its ability to handle blurry boundaries and small-scale vessel features. It is worth noting that MedSAM resizes all inputs to 1024×1024 , potentially offering it a resolution-based advantage in this comparison.

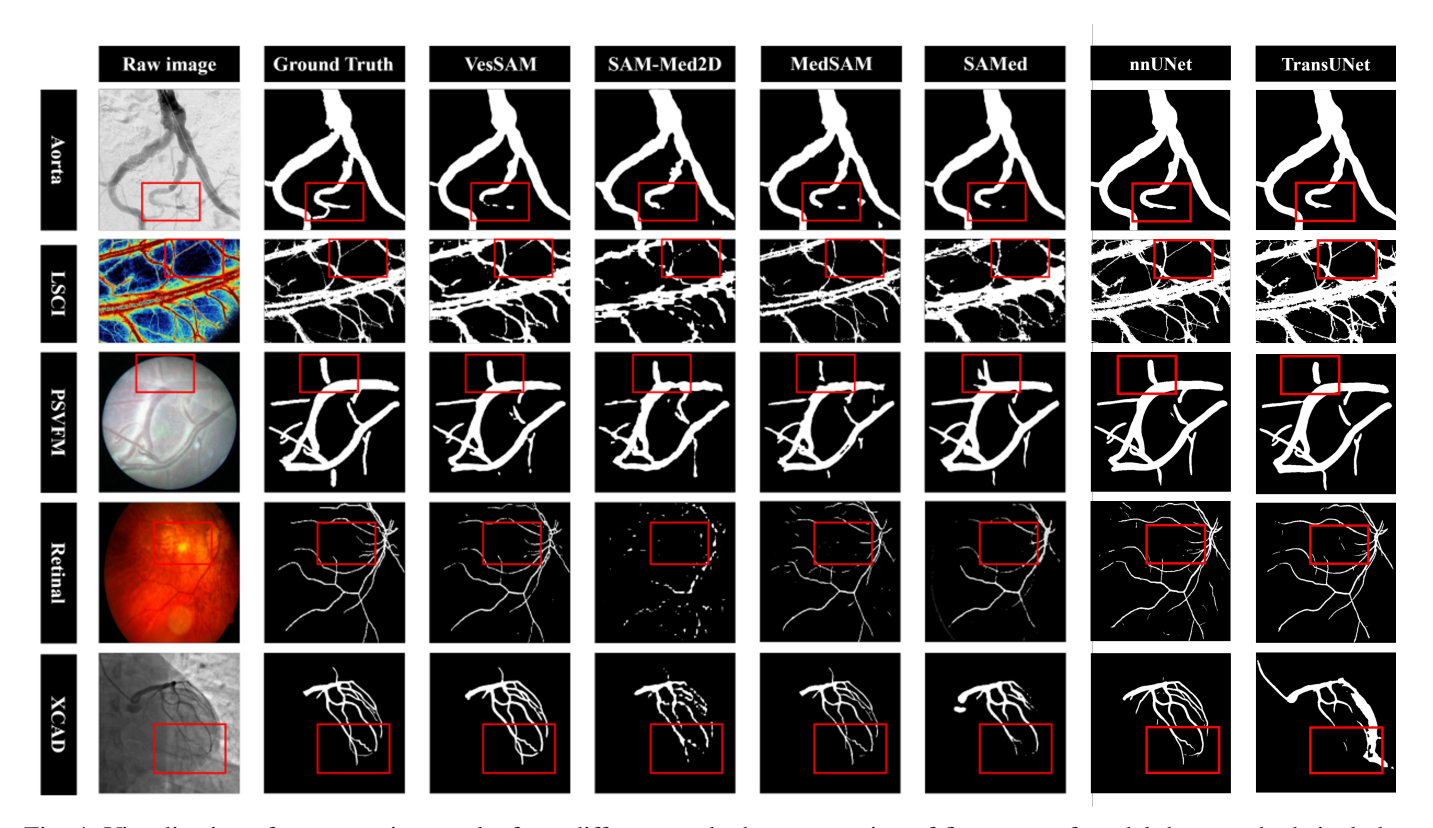


Fig. 4: Visualization of segmentation results from different methods, presentation of five types of modal data, methods include PEFT fine-tuned VesSAM, SAM-Med2D, SAMed, and fully fine-tuned MedSAM, uuUNet, and TransUNet.

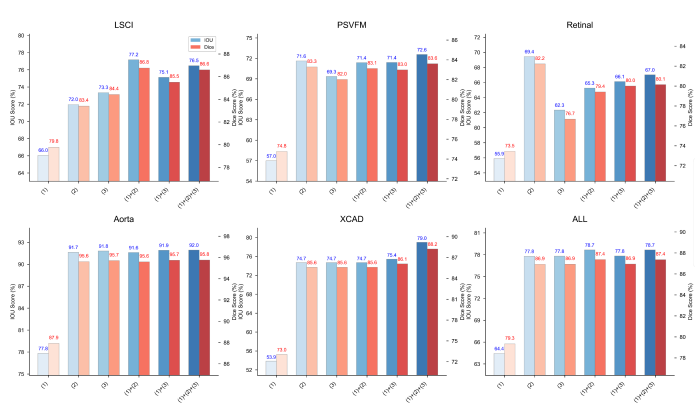


Fig. 5: Ablation study on the effectiveness of different prompt combinations for vessel segmentation. Each bar group represents segmentation performance (Dice and IoU) under varying prompt inputs: (1) branch point prompts only, (2) segment midpoint prompts only, (3) skeleton prompts only, (1)+(2), (1)+(3), and full combination (1)+(2)+(3). Results show that using multiple complementary prompts significantly improves segmentation accuracy, with the full combination consistently achieving the best performance across most datasets.

Performance under Out-of-Distribution (OoD) Settings. To evaluate cross-domain generalization, we conduct experiments under the out-of-distribution (OoD) setting by holding

out one modality as the test domain while training on the remaining ones. As shown in Table II, VesSAM achieves an average Dice score of 61.4% and an IoU of 48.11%, marking an improvement of 9.56% and 9.78% over SAMed, respectively. Compared to other methods, VesSAM exhibits greater resilience on challenging datasets such as Retinal and XCAD, where complex vascular structures and terminal branches require detailed supervision. In contrast, SAM-Med2D, SAMed, nnUNet, and MedSAM suffer substantial performance drops on these datasets, particularly in scenarios involving small vessels and boundary ambiguity. These results underscore the importance of structure-aware prompting in achieving robust generalization across heterogeneous imaging domains.

Visualization Analysis. Qualitative comparisons further highlight VesSAM's strengths. As illustrated in Fig. 6, across five modalities, VesSAM consistently produces smoother and more anatomically accurate vessel masks. For instance, in the Aorta dataset, where noise artifacts resemble vessel endpoints, MedSAM is easily prone to false positives, while VesSAM leverages keypoint prompts to preserve structure and reject irrelevant features. TransUNet and nnUNet, although competitive, often miss thin branches or introduce artifacts in low-contrast regions. VesSAM also outperforms others on the LSCI dataset by effectively suppressing background noise while preserving fine vascular continuity. On PSVFM and XCAD, where boundary quality is compromised, VesSAM

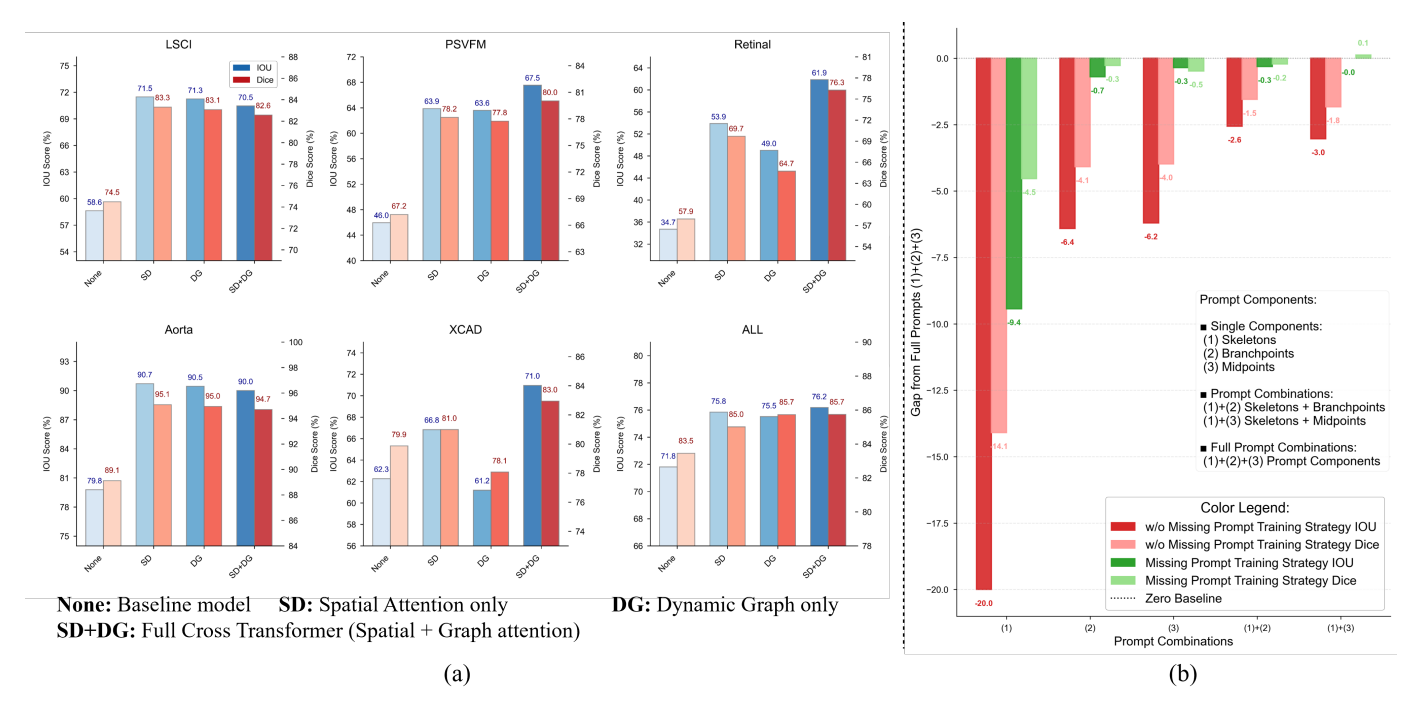


Fig. 6: Ablation results illustrating the effectiveness of prompt feature fusion and the robustness of prompt omission strategies. (a) Comparison of different information fusion schemes in the prompt encoder: using no fusion (None), only sparse-dense (SD), only dense-graph (DG), and both SD and DG simultaneously (SD+DG). The results show that incorporating both fusion types yields the highest segmentation performance. (b) Evaluation of the proposed missing prompt training strategy. Models trained with random prompt omission (as described in Section V) exhibit significantly improved performance when tested with individual missing prompts, especially for weaker prompts like skeleton maps. Both sub-figures use Dice and IoU scores as vertical axes to measure relative performance across prompt conditions.

benefits from stronger prompt encoding and convolutional refinement, yielding sharper and more complete segmentation. In contrast to the jagged artifacts observed in SAM-Med2D outputs, VesSAM's mask decoder produces more consistent and artifact-free results.

Multi-Prompt Ablation Study. To understand the contribution of each type of prompt, we perform extensive ablation experiments across various prompt configurations (Fig. 5). Results indicate that using any single prompt yields limited performance, with skeleton prompts performing the worst when used in isolation. Point prompts (branch points and segment midpoints) achieve moderate improvements individually, and combining point prompts with skeletons provides additional gains. The best results are obtained when all three prompt types are used together, confirming that diverse anatomical cues offer complementary information. Notably, a few configurations with all prompts under-perform slightly due to the stochastic training strategy, where the simultaneous appearance of all prompts is relatively rare, suggesting further room for training schedule optimization.

Information Fusion Ablation. We further ablate the impact of the proposed information fusion modules in the prompt encoder. As shown in Fig. 6(a), removing all fusion mechanisms ("None") results in a performance drop of over 5% (Dice and IoU). Incorporating either sparse-to-dense (SD) or dense-to-

graph (DG) fusion yields moderate improvements, while using both modules in tandem results in the highest performance gain—surpassing the baseline by more than 10% on average. These findings validate the necessity of structured information interaction for effectively integrating diverse prompt features.

Prompt Omission Strategy. To enhance model robustness in real-world scenarios where certain prompts may be unavailable, we propose a stochastic prompt omission strategy during training. As shown in Fig. 6(b), this approach significantly improves performance when individual prompts are missing at inference. In particular, segmentation based solely on skeleton prompts improves by approximately 10% in both Dice and IoU, while point-based prompts also see a minimum improvement of 5%. These results confirm that stochastic training regularization improves the model's ability to handle prompt sparsity, which is crucial for deployment in practical, imperfect annotation environments.

Discussion. The core idea of VesSAM is to leverage high-information anatomical prompts—such as bifurcations and midpoints—to guide segmentation in complex, non-convex structures like vascular networks. Unlike organ segmentation where random prompts suffice, vascular prompts must capture topological continuity and local geometry, offering greater stability across perturbations and modality shifts. Future work may explore automated or learned high-information prompts.

Extending VesSAM to 3D introduces new challenges due to more complex branching and topology. Designing effective prompts and spatial reasoning in 3D, and applying the framework to other non-convex domains like nerves or airways, represent promising directions for generalization.

VII. CONCLUSION

Segmenting non-convex anatomical structures such as blood vessels remains a challenging task for existing methods, due to their intricate morphology and fine-scale features. In this work, we introduce VesSAM, a prompt-aware and parameterefficient segmentation framework tailored for vascular structures. VesSAM comprises three modules: a convolutional adapter for fine-grained texture extraction, a multi-prompt encoder for anatomical fusion, and a lightweight decoder to reduce jagged artifacts. To facilitate practical deployment, we further propose a missing-prompt training strategy to improve robustness under partial supervision. In addition, we also construct a multi-modal benchmark across five modalities and eight datasets, with structured prompts generated via our pipeline. Extensive experiments confirm that VesSAM achieves strong performance and generalization, outperforming both SAM-based PEFT methods and several fully finetuned baselines. Our work connects general foundation models with structure-specific medical tasks, providing a scalable and annotation-efficient solution for complex vascular segmentation. VesSAM marks a promising step toward prompt-driven fine-structure segmentation in biomedical imaging.

REFERENCES

- O. Ronneberger, P. Fischer, and T. Brox, "U-Net: Convolutional networks for biomedical image segmentation," in *Proc. Int. Conf. Med. Image Comput. Comput.-Assist. Intervent. (MICCAI)*, 2015, vol. 9351, pp. 234–241.
- [2] K. He, X. Zhang, S. Ren et al., "Deep residual learning for image recognition," in *Proc. IEEE Conf. Comput. Vis. Pattern Recognit.* (CVPR), 2016, pp. 770–778.
- [3] G. Huang, Z. Liu, L. van der Maaten et al., "Densely connected convolutional networks," in *Proc. IEEE Conf. Comput. Vis. Pattern Recognit. (CVPR)*, 2017, pp. 4700–4708.
- [4] F. Isensee, P. F. Jaeger, S. A. A. Kohl et al., "nnU-Net: A self-configuring method for deep learning-based biomedical image segmentation," *Nat. Methods*, vol. 18, no. 2, pp. 203–211, 2021.
- [5] J. Chen, Y. Lu, Q. Yu et al., "TransUNet: Transformers make strong encoders for medical image segmentation," in arXiv preprint arXiv:2102.04306, 2021.
- [6] Z. Liu, Y. Lin, Y. Cao et al., "Swin transformer: Hierarchical vision transformer using shifted windows," in *Proc. IEEE/CVF Int. Conf. Comput. Vis. (ICCV)*, 2021, pp. 10012–10022.
- [7] A. Dosovitskiy, L. Beyer, A. Kolesnikov et al., "An image is worth 16x16 words: Transformers for image recognition at scale," in arXiv preprint arXiv:2010.11929, 2020.
- [8] V. Zohranyan, M. Haghighi, S. Wang et al., "Dr-SAM: An End-to-End Framework for Vascular Segmentation, Diameter Estimation and Anomaly Detection on Angiography Images," in *Proc. IEEE/CVF Conf.* Comput. Vis. Pattern Recognit. (CVPR), 2024, pp. 5113–5121.
- [9] Y. Ma, M. Liu, S. Huang et al., "Self-supervised vessel segmentation via adversarial learning," in *Proc. IEEE/CVF Int. Conf. Comput. Vis.* (ICCV), 2021, pp. 7536–7545.
- [10] D. J. J. Farnell, A. Papageorgiou, A. S. French et al., "Enhancement of blood vessels in digital fundus photographs via the application of multiscale line operators," *J. Franklin Inst.*, vol. 345, no. 7, pp. 748– 765, 2008.

- [11] J. Staal, M. D. Abramoff, M. Niemeijer et al., "Ridge-based vessel segmentation in color images of the retina," *IEEE Trans. Med. Imag.*, vol. 23, no. 4, pp. 501–509, 2004.
- [12] T. Köhler, F. Maier, A. Hornegger et al., "Automatic no-reference quality assessment for retinal fundus images using vessel segmentation," in Proc. IEEE Int. Symp. Comput.-Based Med. Syst. (CBMS), 2013, pp. 1– 6
- [13] J. Zhang, S. Dashtbozorg, G. P. Looman et al., "Robust retinal vessel segmentation via locally adaptive derivative frames in orientation scores," *IEEE Trans. Med. Imag.*, vol. 35, no. 12, pp. 2631–2644, 2016.
- [14] S. Bano, F. Vasconcelos, L. M. Shepherd et al., "Deep placental vessel segmentation for fetoscopic mosaicking," in *Proc. Int. Conf. Med. Image Comput. Comput.-Assist. Intervent. (MICCAI)*, 2020, vol. 12263, pp. 763–772.
- [15] X. Zhao, R. Vemulapalli, P. A. Mansfield, et al., "Contrastive learning for label efficient semantic segmentation," in *Proc. IEEE/CVF Int. Conf. Comput. Vis. (ICCV)*, 2021, pp. 10623–10633.
- [16] S. Fu, J. Xu, S. Chang et al., "Robust vascular segmentation for raw complex images of laser speckle contrast based on weakly supervised learning," *IEEE Trans. Med. Imag.*, vol. 43, no. 1, pp. 39–50, 2023.
- [17] S. Yao, H. Wu, S. Fu et al., "High-performance laser speckle contrast image vascular segmentation without delicate pseudo-label reliance," J. Innov. Opt. Health Sci., vol. 18, no. 1, 2025.
- [18] K. Yang, S. Chang, J. Yuan et al., "Robust vascular segmentation in laser speckle contrast images based on semi-weakly supervised learning," *Phys. Med. Biol.*, vol. 68, no. 14, Art. no. 145008, 2023.
- [19] A. Vaswani, N. Shazeer, N. Parmar et al., "Attention is all you need," in Adv. Neural Inf. Process. Syst. (NeurIPS), vol. 30, 2017.
- [20] J. Devlin, M.-W. Chang, K. Lee, and K. Toutanova, "BERT: Pre-training of deep bidirectional transformers for language understanding," in *Proc. Conf. North Amer. Chapter Assoc. Comput. Linguist.* (NAACL), 2019.
- [21] H. Touvron, T. Lavril, G. Izacard et al., "LLaMA: Open and efficient foundation language models," in arXiv preprint arXiv:2302.13971, 2023.
- [22] J. Achiam, S. Adler, S. Agarwal et al., "GPT-4 technical report," in arXiv preprint arXiv:2303.08774, 2023.
- [23] GLM Team, A. Zeng, B. Xu et al., "ChatGLM: A family of large language models from GLM-130B to GLM-4 All Tools," in arXiv preprint arXiv:2406.12793, 2024.
- [24] S. Liu, Z. Zeng, T. Ren et al., "Grounding DINO: Marrying DINO with grounded pre-training for open-set object detection," in *Proc. Eur. Conf. Comput. Vis. (ECCV)*, 2024.
- [25] A. Radford, J. W. Kim, C. Hallacy et al., "Learning transferable visual models from natural language supervision," in *Proc. Int. Conf. Mach. Learn. (ICML)*, 2021.
- [26] Z. Yang, L. Li, K. Lin et al., "The dawn of LMMs: Preliminary explorations with GPT-4V(ision)," in arXiv preprint arXiv:2309.17421, 2023.
- [27] A. Ramesh, M. Pavlov, G. Goh et al., "Zero-shot text-to-image generation," in *Proc. Int. Conf. Mach. Learn. (ICML)*, 2021.
- [28] J. Li, D. Li, C. Xiong et al., "BLIP: Bootstrapping language-image pretraining for unified vision-language understanding and generation," in Proc. Int. Conf. Mach. Learn. (ICML), 2022.
- [29] R. Rombach, A. Blattmann, D. Lorenz et al., "High-resolution image synthesis with latent diffusion models," in *Proc. IEEE/CVF Conf. Comput. Vis. Pattern Recognit. (CVPR)*, 2022.
- [30] A. Kirillov, E. Mintun, N. Ravi et al., "Segment anything," in Proc. IEEE/CVF Int. Conf. Comput. Vis. (ICCV), 2023.
- [31] J. Ma, Y. He, F. Li et al., "Segment anything in medical images," *Nat. Commun.*, vol. 15, no. 1, Art. no. 654, 2024.
- [32] K. Zhang and D. Liu, "Customized segment anything model for medical image segmentation," in arXiv preprint arXiv:2304.13785, 2023.
- [33] J. Cheng, J. Ye, Z. Deng et al., "SAM-Med2D," in arXiv preprint arXiv:2308.16184, 2023.
- [34] H. Wang, S. Guo, J. Ye et al., "SAM-Med3D: Towards general-purpose segmentation models for volumetric medical images," in *European Conference on Computer Vision (ECCV)*, 2024.
- [35] C. Chen, J. Miao, D. Wu et al., "MA-SAM: Modality-agnostic SAM adaptation for 3D medical image segmentation," *Med. Image Anal.*, vol. 98, Art. no. 103310, 2024.
- [36] S. Gong, Y. Zhong, W. Ma et al., "3DSAM-adapter: Holistic adaptation of SAM from 2D to 3D for promptable tumor segmentation," *Med. Image Anal.*, vol. 98, Art. no. 103324, 2024.

- [37] J. Zhu, Y. Qi, and J. Wu, "Medical SAM 2: Segment medical images as video via segment anything model 2," in arXiv preprint arXiv:2408.00874, 2024.
- [38] E. J. Hu, Y. Shen, P. Wallis, et al., "LoRA: Low-rank adaptation of large language models," in *Proc. Int. Conf. Learn. Representations (ICLR)*, 2022.
- [39] M. Jia, L. Tang, B. C. Chen, et al., "Visual prompt tuning," in Proc. Eur. Conf. Comput. Vis. (ECCV), 2022, pp. 709–727.
- [40] Z. Chen, Y. Duan, W. Wang, et al., "Vision transformer adapter for dense predictions," arXiv preprint arXiv:2205.08534, 2022.
- [41] Y. Xin, S. Luo, H. Zhou, et al., "Parameter-efficient fine-tuning for pre-trained vision models: A survey," arXiv preprint arXiv:2402.02242, 2024
- [42] Z. Han, C. Gao, J. Liu, et al., "Parameter-efficient fine-tuning for large models: A comprehensive survey," arXiv preprint arXiv:2403.14608, 2024.
- [43] H. Liu, C. Li, Q. Wu, et al., "Visual instruction tuning," in Adv. Neural Inf. Process. Syst. (NeurIPS), vol. 36, pp. 34892–34916, 2023.
- [44] J. Lee, W. Yoon, S. Kim, et al., "BioBERT: A pre-trained biomedical language representation model for biomedical text mining," *Bioinfor-matics*, vol. 36, no. 4, pp. 1234–1240, 2020.
- [45] Z. Kraljevic, A. Shek, D. Bean, et al., "MedGPT: Medical concept prediction from clinical narratives," arXiv preprint arXiv:2107.03134, 2021.